IOSR Journal of Applied Physics (IOSR-JAP)
e-ISSN: 2278-4861.Volume 11, Issue 4 Ser. I (Jul. – Aug. 2019), PP 01-21
www.iosrjournals.org

Comparative Study Between Moth Flame And Ant-Lion Optimization Techniques Using Parameter Extraction Of A Three Diode Model Of A Photovoltaic Module.

[1]A. M. Nura,[2]S.A. Muhammad
[1]*Department of Physics Bayero University, Kano - Nigeria.*
[2]*Government Sec. Sch. Gadadin Dutse, Jigawa State - Nigeria.*

Abstract: *This paper evaluated and compared the performance of two recently developed optimization algorithms: Moth-Flame Optimization (MFO) and Antlion Optimization (ALO) using parameter extraction of a Three Diode Model (TDM) of a photovoltaic module. These techniques were equally recently reported to have good performance. However, it is imperative to know the best method among them in terms of accuracy, execution time and speed of convergence for a given optimization problem. Experiments were conducted to obtain several values for the PV module's currents and voltages. Part of the data were used in optimizing the TDM parameters by the two optimization techniques using MATLAB R2017a programming software. The remaining data were used to validates the two codes. The performances of the two techniques in terms of the speed convergence, execution time and accuracy were compared through I-V curve fitting approach and statistical analysis such as Mean Bias error (MBE) and Absolute Error at Maximum Power Point (AE at MPP). The results show that MFO has better performance in terms of both accuracy and speed of execution with average value of MBE as 0.15, AE at MPP as 0.02 and ET as 152.2288 sec than the ALO with MBE of 0.17, AE at MPP of 0.14 and ET of 2254.1822 sec, indicating that the MFO is 93.24% faster than the ALO. Other statistical parameters evaluated agree with these findings. The MFO was found to outperform the ALO in terms of speed of convergence.*

Keywords: *Ant-lion Optimization (ALO), Moth Flame Optimization (MFO), Three Diode Model (TDM).*

Date of Submission: 22-06-2019 Date of acceptance: 05-07-2019

I. Introduction

Solar energy is the most readily available source of energy that is free. It is a renewable energy source that will contribute to secure future energy demands without emission of pollutants items to air and our environment. Solar energy can be converted to electricity using photovoltaic (PV) cells. The PV cells are p-n junction semiconductor devices that work under the principle of photoelectric effect. The power produced by a single PV cell is not enough for general use, as such several PV cells are connected to form photovoltaic modules and several modules can be connected to form photovoltaic array [1]. The most efficient PV cell produced was reported to have efficiency of 46.0±2.2% [2]. Due to the lower output efficiency of the PV cell, enormous amount of work has been carried out to physically improve their performance [3], [4]. However, it appears that a proper system design also plays a significant role in increasing the overall efficiency of photovoltaic systems. Thus, several models were designed to predict the real behavior of the PV cell under varying environmental conditions to improve their performance.

The objective of the models is to emulate the electrical behavior of physical PV modules [5]. The popular approach is to utilize electrical equivalent circuit model [6] which is primarily based on an independent light generated current source connected in parallel to a p-n junction diode. Many models have been proposed for the simulation of the PV cells [7]. The complexity ranges from the simplest model which is the Single Diode Model (SDM) and passing through the more elaborate models such as the Double Diode Model (DDM) and to the more detailed models such as the Three-diode model (TDM). To implement these model's various electrical parameters must be evaluated which include; photocurrent (Iph) representing the independent light generated current source, diode reverse saturation current (Io), diode ideality factor (a), series resistance (Rs) and shunt resistance (Rp).

Because of the transcendental nature of the different model's equation, these parameters cannot be solved explicitly [6]. However, several conventional and heuristic techniques were used to extract the parameters for the last few decades [8]. Some of the recent literature based on these two techniques include: For the conventional techniques, the recent research include [9][10]. For the heuristic, recently the following techniques were used: Genetic Algorithm (GA) [11]–[14], Simulated Annealing (SA) [15], [16]), Particle

Swarm Optimization (PSO) [17], [18], Differential Evolution [6], [19]–[21], Firefly Algorithm (FF) [22], Gravitational Search Algorithm (GSA) [23], Antlion Optimization (ALO) [24], Hybrid genetic Algorithm [12], Pattern Search Technique (PS) [25], and Moth Flame Optimization (MFO) [26]. The heuristic methods have shown better precision and computational efficiency as compared to the conventional methods [17].

From the literature it is observed that, several research investigations on PV cell models' parameters extraction was carried out but very few researchers investigated the TDM based on outdoor experimental I-V data set. Ref [8]reviewed over 100 published available researches conducted from 2011 to 2017 on PV cell models' parameters extraction out of which very few groups of researchers investigated the TDM. Ref.[26] extracted seven out of the nine unknown electrical parameters of the TDM based on laboratory measured I-V data set taken using solar simulator. Also, ref. [17]extracted TDM with variable resistance parameters using I-V data set taken using laboratory I-V measurement system. According to [26] some of the researchers relied on conventional algorithms, which were proven to suffer from inaccuracy with the increased number of the unknown parameters and take longer execution time. However, the increase in number of the unknown electrical parameters of the TDM make most of the techniques to lose their accuracy. Thus, more efficient and powerful optimization techniques should be introduced to estimate the TDM parameters base on real outdoor experimental I-V data with accuracy and within shortest execution time.

This paper compared the performance of two recently developed meta-heuristic optimization techniques: MFO and ALO in terms of accuracy, execution time and speed of convergence using TDM parameter extraction optimization problem based on real outdoor experimental I-V data by extracting the complete nine unknown electrical parameters of the model. The two techniques were recently reported to have good performance when applied for the PV cell models' parameters extraction problem based on I-V data set taken using laboratory I-V measurement system [24], [26].The accuracy of the techniques was evaluated using I-V curve fitting approach and statistical relations namely; Root Mean Square Error (RMSE), Mean Bias Error (MBE), Absolute Error at Maximum Power Point (AE at MPP) and Coefficient of Determination (R^2). The speed of the techniques was evaluated in terms of execution time ET and rate of convergence.

II. Background Theory

Photovoltaic cell working principle is based on photoelectric effect were absorption of a photon leads to generation of electron-hole pairs. These electron-hole pairs are likely to recombine to lose their electrical energy but the built in potential barrier of the PV cell separate them, sending more holes to one side of the cell and more electron to the other. These charge separation sets up a voltage difference between either ends of the cell which can be used to derive an electric current in an external circuit. Modeling is required to predict the behavior of PV cell under varying environmental conditions. The popular approach is to utilize electric equivalent circuit model. The complexity ranges from single diode model to the double and three diode models.

The SDM is based on an equivalent circuit consisting of an independent current source represented by photocurrent (I_{ph}) connected in parallel with a diode (D), a shunt resistance (R_p) and a series resistance (R_s) [27]. The Diode current I_d represents the current due to diffusion, the series resistance R_s represents the resistance in the path of the current due to contact resistances and resistance in the emitter and bulk regions and Shunt resistance R_p represents the current leakage across the p-n junction of the PV module [17]. This model assumes that, the recombination losses in the depletion regions are absent. Consideration of these losses leads to the DDM [28].The DDM is more precise than the SDM because the effect of the recombination loss in the depletion region was considered which is modeled by the second diode. The DDM has some limitations whereby, the output performance is still not appreciable because of the effect of recombination of electron-hole pair in the defect region. Considering this loss leads to an improved model known as the TDM with additional diode in parallel to the other two [17].

2.1 Three Diode Model

The purpose of adding a third diode in parallel to the two diodes in TDM is to consider contribution of the diode current component (I_{D3}) due to recombination in the defect regions [17]. Fig.1 depict the TDM equivalent circuit.

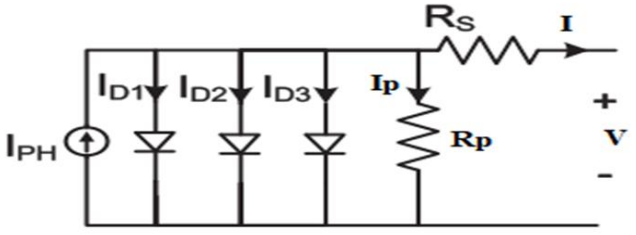

Figure 1. Three Diode Equivalent Circuit Model.

The series resistance R_s and Shunt resistance R_p are the same resistance components as defined for SDM and DDM. The current through the circuit elements in Fig. 1 is governed by the voltage across them expressed as (1):

$$Va = V + IR_s \quad (1)$$

where; Va is the voltage across both diodes and shunt resistance, R_s is the series resistance, I is the output current and V is voltage across the output terminals.

Considering the loop of the voltage V across the series resistanceR_S and the shunt resistance R_p in Fig. 1, the shunt current I_p can be expressed as (2):

$$I_p = \frac{V+IR_s}{R_p} \quad (2)$$

For a given irradiance and temperature, the I–V relationship for the circuit in Fig. 1 can be represented by applying Kirchhoff's current rule as;

$$I_{ph} = I_{D1} + I_{D2} + I_{D3} + I_p + I \quad (3)$$
$$I = I_{ph} - I_{D1} - I_{D2} - I_{D3} - I_p \quad (4)$$

where I_{D1}, $I_{D2}$and $I_{D3}$are the diodes currents 1,2 and 3 for the three diodes respectively. I_p is the current through the shunt resistance. The diodes currents are expressed by Shockley equation as follows [29].

$$I_{D1} = I_{01}\left[\exp\left(\frac{V+IR_s}{a_1V_t}\right) - 1\right] \quad (5)$$
$$I_{D2} = I_{02}\left[\exp\left(\frac{V+IR_s}{a_2V_t}\right) - 1\right] \quad (6)$$
$$I_{D3} = I_{03}\left[\exp\left(\frac{V+IR_s}{a_3V_t}\right) - 1\right] \quad (7)$$

where; $I_{01}, I_{02}, I_{03}$are the diode reverse saturation current 1, 2 and 3 in Ampere [A] respectively, V is the voltage across the output terminal of the PV module in Volt [V], $a_1, a_2\ and\ a_3$ are the diode ideality factors 1, 2 and 3. R_S is the series resistance in Ohms [Ω] and V_t is the thermal voltage given by (8).

$$V_t = \frac{kT}{q} \quad (8)$$

where k is the Boltzmann constant in Joules per Kelvin [J/K], T is the temperature of the p-n junction in Kelvin [K] and q is the charge of an electron in Coulomb [C].

With the preceding information, the I-V characteristic equation describing the TDM can now be expressed as;

$$I = I_{ph} - I_{01}\left[exp\left(\frac{V+IR_s}{a_1V_t}\right) - 1\right] - I_{02}\left[exp\left(\frac{V+IR_s}{a_2V_t}\right) - 1\right] - I_{03}\left[exp\left(\frac{V+IR_s}{a_3V_t}\right) - 1\right] - \frac{V+IR_s}{R_p} \quad (9)$$

where; R_p is the shunt resistance in Ohms [Ω] and $I_{ph}$is the independent current source (Photocurrent).

The TDM parameters to be optimized by the proposed optimization techniques are;I_{ph}, R_S, R_p, I_{01}, I_{02}, I_{03}, a_1, a_2 and a_3.

2.2 Problem Formulation

The main requirements to apply the ALO and MFO optimization techniques are accomplished by the determination of the solution vector (X), the search range and the objective function.

2.2.1 The Solution Vector and Search Range

The solution vector is the vector that contains the set of all the parameters to be optimized which can be expressed in this study from (9) as

$$X = [R_s, R_p, I_{o1}, I_{o2}, I_{o3}, a_1, a_2, a_3, I_{ph}]. \quad (10)$$

The search ranges are the boundaries within which the optimal values of the parameters will be looked up.

According to the previous literature the search range of the parameters are selected as follows: $R_p \epsilon [R_{po}$ 5000], $a_{1,2,3} \epsilon$ [0.5 4], $R_s \epsilon$ $[R_{so}$ 2], and $I_{ph} \epsilon$ [0 $2I_{sc}$] where I_{sc} is the short circuit current [20]. $I_{o1,02,03} \epsilon$[0 1e-12] [26]. According to [30]I_{o2} is 3 - 7 orders of magnitude greater than I_{o1}. The values of R_{so} is zero [20] and R_{po} can be evaluated at Standard Test Condition (STC) based on the PV module manufacturers data sheet specifications [20].

$$R_{po} = \frac{V_{MP}}{I_{sc} - I_{MP}} - \frac{V_{OC} - V_{MP}}{I_{MP}} \quad (11)$$

where; V_{OC} is the open circuit voltage, I_{SC} is the short circuit current, I_{MP} is the maximum power current and V_{MP} is the maximum power voltage.

2.2.2 The Objective Function.

The extraction performance is evaluated using objective function formulated as the root mean square of the difference between the measured and simulated model current data for both the two optimization techniques. The difference between the measured and simulated PV module current data is given by the error function $f(V, I, X)$ expressed as;

$$f(V, I, X) = I_L - I_{L-EXP} \quad (12)$$

where the estimated current I_L can be calculated using (9) and I_{L-EXP} is the measured current obtained from the experiment.

Root Mean Squared Error is used as a criterion to express the difference between the measured data and the simulated result. The parameters are extracted by minimizing the Root Mean Squared Error (13).

$$RMSE = \sqrt{\frac{1}{K}\sum_{L=1}^{K} f(V_L, I_L, X)^2} \quad (13)$$

Hence, the objective function for K number of measured I-V data set is defined by (14).

$$\text{Objective function} = min\sqrt{\frac{1}{K}\sum_{L=1}^{K} f(V_L, I_L, X)^2} \quad (14)$$

Smaller value of (14) implies the deviation between the module measured current and the current computed from the extraction method is small. Ideally, a zero value of (14) is desired [20].

2.3 MFO Algorithm

MFO is a new population based algorithm developed by Mirjalili [31] and was inspired by the navigation method of moths in nature called transverse orientation. Moths are fancy insects, they have special navigation methods at night called transverse orientation [31]. In this mechanism, they fly at night by maintaining a fixed angle with respect to the moon, this method is very helpful for traveling in a straight line especially when the light source is very far Fig.2, [31].

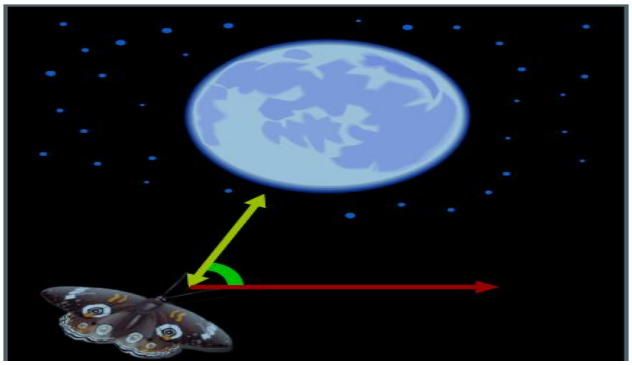

Figure 2 Transverse orientation.

When the light source is close, moths fly spirally around it and finally converge toward it after just a few corrections as shown in Fig.3[31].

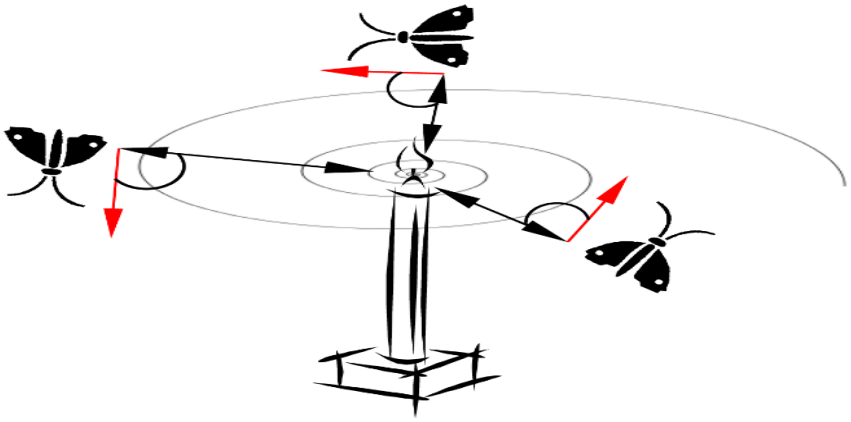

Figure 3 Spiral flying path around close light sources [31].

The key components in the MFO algorithm are moths and flames where both are considered as a solution, however, they differ in the way of their treatment and their updating in each iteration. The moths are actual search agents that move around the search space, while flames are the best position of moths that are obtained so far. Thus, flames can be considered as flags that are dropped by moths when searching the search space. Therefore, each moth searches around a flag and updates it in case of finding a better solution [31]. Since the MFO algorithm is a population-based algorithm, the set of moths and flames can be represented in a matrix given by (15) and (16) respectively [31].

$$M = \begin{bmatrix} m_{1,1} & m_{1,2} & \dots & \dots & m_{1,d} \\ m_{2,1} & m_{2,2} & \dots & \dots & m_{2,d} \\ \vdots & \vdots & \vdots & \vdots & \vdots \\ m_{n,1} & m_{n,2} & \dots & \dots & m_{n,d} \end{bmatrix} \quad (15)$$

$$F = \begin{bmatrix} F_{1,1} & F_{1,2} & \dots & \dots & F_{1,d} \\ F_{2,1} & F_{2,2} & \dots & \dots & F_{2,d} \\ \vdots & \vdots & \vdots & \vdots & \vdots \\ F_{n,1} & F_{n,2} & \dots & \dots & F_{n,d} \end{bmatrix} \quad (16)$$

where; n is the number of moths and d is the number of variable.

For both the moths and flames there is an array for storing their corresponding fitness values each as follows [31].

$$OM = [OM_1 \quad OM_2 \dots \quad OM_n]^{\mathrm{T}} \quad (17)$$

$$OF = [OF_1 \quad OF_2 \dots \quad OF_n]^{\mathrm{T}} \quad (18)$$

where n is the number of moth and $_{\mathrm{T}}$ is transpose.
The general structure of the MFO algorithm contains three-tuple approximation functions that are summarized as follows [31].

$$MFO = (I, P, T) \quad (19)$$

The I function: The '*I*' is the initialization function that generates a random population of moths using (20) and stored in (15) and evaluate their corresponding fitness values using (14) and stored in (16).

$$M(i,j) = \big(ub(i) - lb(i)\big) * rand() + lb(i) \quad (20)$$

where ub and lb are upper and lower bound of the variables respectively, $rand$ is a random number between 0 and 1.

***The P function*:** The '*P*' is the main function which moves the moths around the search space and receive the matrix 'M' (15) and returns its updated one eventually.
After initialization, the P function is iteratively run until the termination function *T* is satisfied. As mentioned earlier, the inspiration of this algorithm is the transverse orientation of moth. Thus, in order to mathematically model this behavior, a logarithmic spiral is chosen as the update mechanism of the position of each moths with respect to the flame [31].The position of each moths is updated with respect to a flame using (21) [31].

$$M_i = S(M_i, F_j) \qquad (21)$$

The logarithmic spiral for the Moth Flame optimization algorithm is defined by (22).

$$S(M_i, F_j) = D_i * e^{bt} * \cos(2\pi t) + F_j \qquad (22)$$

where M_i indicate the $i-th$ moth, Fj indicates the$j-th$ flame, and S is the spiral function. D_i indicates the distance of the $i-th$ moth for the $j-th$ flame, b is a constant for defining the shape of the logarithmic spiral, and t is a random number in [r, 1]. Adaptive convergence constant r linearly decreases from -1 to -2 to accelerate convergence around the flames over the course of iterations. The lower the t, the closer the distance to the flame [31].

The distance of the i-th moth for the j-th flame $D_i$can be evaluated using (23) as follows;

$$D_i = |F_j - M_i| \qquad (23)$$

(22) is where the spiral flying path of moths is simulated. The next position of a moth is defined with respect to a flame. The t parameter in the spiral equation defines how much the next position of the moth should be close to the flame ($t = -1$ is the closest position to the flame while $t = 1$ is the furthest).

The logarithmic spiral, space around the flame, and the position considering different t on the curve are illustrated in Figure 4.

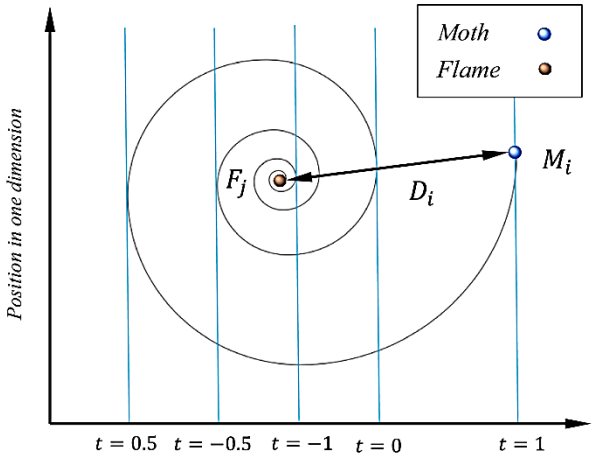

Figure 4 Logarithmic spiral, space around the flame and the position with respect to t [31]

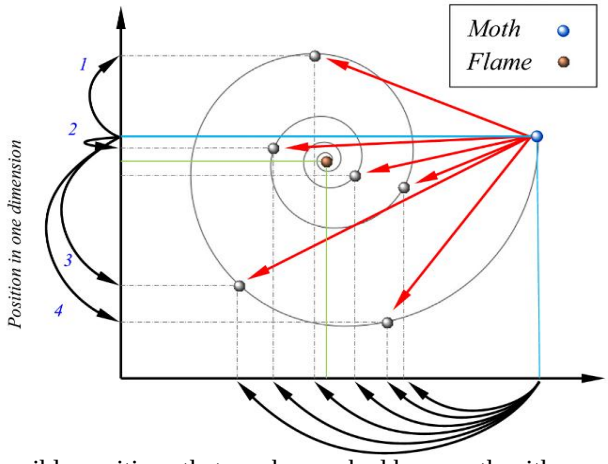

Figure 5 Some of the possible positions that can be reached by a moth with respect to a flame using the logarithmic spiral [31].

The spiral equation allows a moth to fly around a flame and not necessarily in the space between them. Fig. 5 illustrates the updated moth positions around the flame. Exploration occurs when the next position lies outsides the space between the moth and the flame as illustrated in the arrows labeled 1,3 and 4 in Fig. 5. Exploitation happens when the next position lies inside the space between the moth and the flame as observed in the arrow labeled 2 in Fig. 5.

To balance between the exploration and exploitation, the number of flames adaptively decreases over the iterations as given in (24) [31].

$$flame\ no. = round\left(N - l * \frac{N-1}{T}\right) \quad (24)$$

where; l is the current number of iteration, N is the maximum number of flames, and T is the maximum number of iterations.
However, the moth updates their position only with respect to the best flame in the final step of the iterations. The gradual decrement in number of flames balances exploration and exploitation of the search space [31].
***The termination function T*:** The p function is executed until the T function is satisfied. Therefore, after the termination of the P function, the best moth is returned as the best obtained approximation of the optimum [31]

2.4 ALO Algorithm

The antlion optimizer is a recently developed meta-heuristic nature inspired algorithm developed by Mirjalili in 2015 [32] which imitates the hunting strategy of antlions in nature for catching ants. Antlions are insects that exhibit two phases in their life cycle namely; larvae and adult. In larvae stage, they hunt insects

especially ants, whereas, adult stage is meant for breeding. Antlion larvae dig a cone-shaped pit by moving around in a circular path as illustrated in Fig. 6.

The Antlion hides underneath the bottom of the cone shaped pit and waits for the ants to be trapped in the pit. When an ant happens to pass over the pit, it slides and falls inside the trap. Antlion tries to catch the ant when it realizes the ant is trapped.

Figure 6 Antlion cone shape pit.

However, ants usually try to get away from the trap as such antlion shoot sand at the edge of the trap to slide the ant to the bottom and then catches it as illustrated in Fig. 7. After consuming the prey, antlions re-build the trap [32].

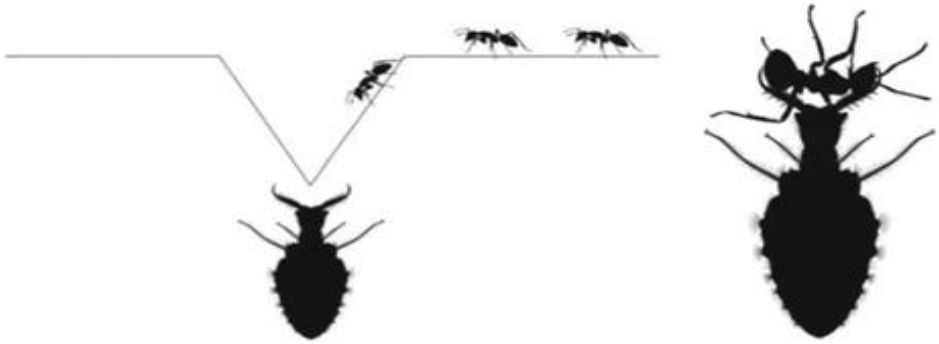

Figure 7 Antlion hides underneath the bottom of its cone-shaped pit waiting for ant [24].

Since the ALO algorithm is a population-based algorithm, the positions of ants are saved in matrixM_{Ant} given by (25) where $A_{i,j}$ denotes the j-th dimension position of the j-th variable of i-th ant [32].

$$M_{Ant} = \begin{bmatrix} A_{1,1} & A_{1,2} & \dots & \dots & A_{1,d} \\ A_{2,1} & A_{2,2} & \dots & \dots & A_{2,d} \\ \vdots & \vdots & \vdots & \vdots & \vdots \\ A_{n,1} & A_{n,2} & \dots & \dots & A_{n,d} \end{bmatrix} \quad (25)$$

The fitness of ants is saved in matrix M_{OA} given by (26) [32].

$$M_{OA} = \begin{bmatrix} f(A_{1,1} & A_{1,2} & \dots & \dots & A_{1,d}) \\ f(A_{2,1} & A_{2,2} & \dots & \dots & A_{2,d}) \\ \vdots & \vdots & \vdots & \vdots & \vdots \\ f(A_{n,1} & A_{n,2} & \dots & \dots & A_{n,d}) \end{bmatrix} \quad (26)$$

Similarly, the positions of antlions are saved in a matrix $M_{Antlion}$ given by (27) where $AL_{i,j}$, denotes the j-th dimension position of the i-th antlion [32].

$$M_{Antlion} = \begin{bmatrix} AL_{1,1}AL_{1,2} \dots & \dots & AL_{1,d} \\ AL_{2,1} \; AL_{2,2} & \dots & \dots \; AL_{2,d} \\ \vdots \quad \vdots & \vdots & \vdots \quad \vdots \\ AL_{n,1}AL_{n,2} & \dots & \dots \; AL_{n,d} \end{bmatrix} (27)$$

The fitness of antlion is saved in matrix M_{OAL} given by (28).Among them, elite individual is the antlion with the best fitness [32].

$$M_{OAL} = \begin{bmatrix} f(AL_{1,1}AL_{1,2} \dots & \dots & AL_{1,d}) \\ f(AL_{2,1} \; AL_{2,2} & \dots & \dots \; AL_{2,d}) \\ \vdots \quad \vdots & \vdots & \vdots \quad \vdots \\ f(\; AL_{n,1}AL_{n,2} & \dots & \dots \; AL_{n,d}) \end{bmatrix} (28)$$

The ALO algorithm is defined as a three-tuple function that approximates the global optimum for optimization problems as $ALO(A, B, C)$[32].

The function *A*: This function generates the random initial population of ants and antlions stored in a matrix given by (25) and (27) respectively with their corresponding fitness values stored in a matrix given by (26) and (28) respectively. The initialization function is given by (28) [32].

$$M(i,j) = \big(ub(i) - lb(i)\big) * rand() + lb(i) \qquad (29)$$

where ub and lb are the lower and upper bounds of the parameters.

The function *B*: This function manipulates the initial population provided by the function *A*. The function is described by the following steps;

1). Building the trap: To model the antlions' hunting capability, a roulette wheel is employed[32]. Ants are assumed to be trapped in only one selected antlion. The ALO algorithm is required to utilize a roulette wheel operator for selecting antlion for every ant based on their fitness during optimization [32].

2). Random walk of ant: The movement of ants are stochastic in nature while searching for food. The Random walk of ants is mathematically formulated with (30) [32].

$$X(t) = [0, comsum(2r(t_1) - 1),\ comsum(2r(t_2) - 1),\ \dots, comsum(2r(t_n) - 1)] \qquad (30)$$

where cumsum calculates the cumulative sum, n is the maximum number of iteration, t shows the step of random walk (iteration in this study), and r(t) is a stochastic function defined by (31) [32].

$$r(t) = \begin{cases} 1 \; if \; rand > 0.5 \\ 0 \; if \; rand \; \leq 0.5 \end{cases} \qquad (31)$$

where; t shows the step of random walk and $rand$ is arandom number generated with uniform distribution in the interval of [0, 1][32].

To keep the random walks inside the search space, they are normalized (min–max normalization) as follow [32].

$$R_i^t = \frac{(X_i^t - a_i) \times (d_i - c_i^t)}{(d_i^t - a_i)} + a_i \quad (32)$$

where: R_i^t is the normalized displacement, X_i^t is the random displacement of the i-th Ant in the t-th iteration,$a_i$is the minimum displacement of random walk of i-th variable, $d_i$is the maximum displacement of random walk in i-th variable, $c_i^t$is the minimum displacement of i-th variable at t-th iteration, and d_i^t indicates the maximum displacement of i-th variable at t-th iteration.

***3). Trapping of ants in antlion's pit*:** Random walks of ants are affected by antlions' traps. To model this assumption, (33) and (34) are proposed [32].

$$c_i^t = Antlion_j^t + c^t \quad (33)$$
$$d_i^t = Antlion_j^t + d^t \quad (34)$$

where c^t is the minimum of all variables at t-th iteration, d^t indicates the vector including the maximum of all variables at t-th iteration, c_i^t is the minimum displacement of all variables for i-th ant, d_i^t is the maximum displacement of all variables for i-th ant, and $Antlion_j^t$ shows the position of the selected j-th antlion at t-th iteration. (33) and (34) show that Ants randomly walk in a hyper sphere defined by the vectors c and d around a selected Antlion [32].

4). Sliding of ants towards antlion: Antlions shoot sands outwards the center of the pit once they realize that an Ant is in the trap. This behavior slides down the trapped Ant that is trying to escape. For modeling this behavior, the radius of Ant's random walks hyper-sphere is decreased adaptively c^t and d^t can be evaluated using (35) and (36) [32].

$$c^t = \frac{c^t}{I} \quad (35)$$
$$d^t = \frac{d^t}{I} \quad (36)$$

where; c^t is the minimum of all variables at t-th iteration, and d^t indicates the vector including the maximum of all variables at t-th iteration. The value of I can be evaluated using (37) as;

$$I = 10^W \frac{t}{T} (37)$$

where; t is the current iteration, T is the maximum number of iterations, and w is a constant defined based on the current iteration as (w = 2 when t > 0.1T, w = 3 when t > 0.5T, w = 4 when t > 0.75T, w = 5 when t > 0.9T, and w = 6 when t > 0.95T). Basically, the constant w can adjust the accuracy level of exploitation.

5). Catching prey and re-building the pit: It is assumed that catching prey occur when Ants becomes fitter (goes inside sand) than its corresponding Antlion. Antlion is then required to update its position to the latest position of the hunted Ant to enhance its chance of catching new prey using the Eq. (38) [32].

$$Antlion_j^t = Ant_i^t \ \ if\ f(Ant_i^t) > f(Antlion_j^t) \quad (38)$$

where t shows the current iteration,$Antlion_j^t$ shows the position of selected j-th Antlion at t-th iteration, and Ant_i^t indicates the position of i-th ant at t-th iteration.

6). Elitism: The best Antlion obtained so far in each iteration is saved and considered as an elite. Since the elite is the fittest Antlion, it should be able to affect the movements of all the Ants during iterations. Therefore, it is assumed that every Ant randomly walks around a selected Antlion by the roulette wheel and the elite simultaneously as given by (39) [32].

$$Ant_i^t = \frac{R_A^t + R_E^t}{2} \quad (39)$$

where R_A^t is the random walk around the Antlion selected by the roulette wheel at t-th iteration, $R_E^t$is the random walk around the elite at t-th iteration, and Ant_i^t indicates the position of i-th Ant at t-th iteration.

The function *C:* The B function is executed until the C function is satisfied [32] i.e. true or false.

III. Methodology

To implement the MFO and ALO techniques measured I-V data sets from the PV module along with measuredtemperature and irradiance are required. To obtain these parameters, outdoor experiments were conducted at Bayero University, Kano (latitude 11.97863N, longitude 8.47178E) for a period of ten days. The materials used for the experiment were: Sunshine AP-PM-20 (20W) polycrystalline PV module, digital multimeter with PC interface (MY64-345), Rheostat (SR45,2A and 26Ω), cell temperature detector, solar meter (tpi510) and connecting wires. Fig.8 depicts the experimental set-up.

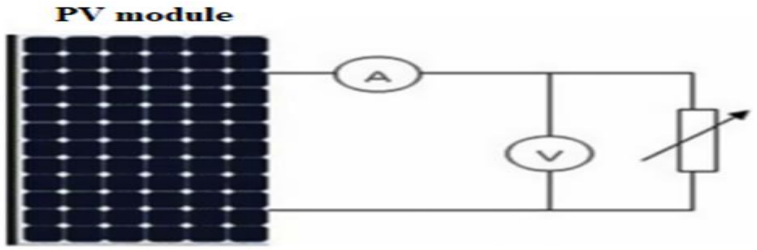

Figure 8 Non Ideal PV Circuit Diagram of the experimental Set-up [33].

3.1 Experimental Procedure

The open circuit voltage (Voc) and short circuit current (Isc) were obtained by opening and shortening the terminals of the set-up. The Rheostat was varied between the Voc and Isc values and the corresponding currents and voltages were recorded. For each experiment the date, time, temperature and irradiances were also recorded. The measured I-V data from the PV module were used for the optimization of the three diode model's parameters of the PV module in a MATLAB R2017a environment.

3.2 Optimization / Simulation

After many runs have been performed, the maximum number of iterations were chosen to be T = 500. The population size N was chosen to be 50. The population size N ranges between [5d 10d] where d is the number of the parameters [26].

3.3 Statistical Analysis

To ensure the proposed algorithms extracted the unknown parameters accurately, a deeper analysis such as Mean Bias error (MBE), Absolute Error (AE) at Maximum Power Point, Root Mean Square Error (RMSE) and Coefficient of Determination (R^2) were carried out.

1). The MBE is a statistical quantity which measures the performance of the ALO and MFO techniques given by (39).

$$MBE = \frac{1}{K}\sum_{i=1}^{k}\left(I_e - I_{exp}\right) \qquad (40)$$

where k is the number of the readings of the measured I-V data and I_e, I_{exp} are the estimated and the experimental currents respectively [26].

*2).*The R^2 was used as a guideline in measuring the accuracy of each technique. R^2 has values between 0 and 1. When its value is 1, it means there is consistency between simulation and experimental result otherwise there is no consistency [26].

$$R^2 = 1 - \frac{\sum_{i=1}^{k}(I_e - I_{exp})^2}{\sum_{i=1}^{k}(I_{exp} - \overline{I_{exp}})} \qquad (41)$$

where: I_e is the estimated current, I_{exp} is the experimental current, k is number of measured data and $\overline{I_{exp}}$: is the arithmetic mean of the experimental current for 'k' number of measured I-V data given by (42).

$$\overline{I_{exp}} = \frac{1}{k}\sum_{i=1}^{k} I_{exp} \qquad (42)$$

3). The Root mean square error analysis was also computed to measure the accuracy of the ALO and MFO techniques and it is defined by (43)

$$RMSE = \sqrt{\frac{1}{k}\sum_{i=1}^{k}(I_e - I_{exp})^2} \qquad (43)$$

where k is the number of the readings of the measured I-V data and I_e, I_{exp} are the estimated and the experimental currents respectively.

*4).*Absolute Error (AE) at maximum power point was also computed using (44) as follows;

$$AE = (I_e - I_{exp}) \qquad (44)$$

where; I_e and I_{exp} are the estimated and experimental currents respectively.

IV. Results and Discussion

Comparison of calculated and measured I-V curves for the AP-PM-20 (20W) Polycrystalline PV module was carried out for the TDM using the MFO and ALO algorithms in order to illustrate the accuracy of the extracted parameters. The parameters of the model were estimated by fitting of the calculated I-V curves to the measured I-V curves with the least achievable MBE, RMSE and AE at MPP as shown in Fig. 9 to 14. This is in contrast to [6] in which no statistical relations were used.

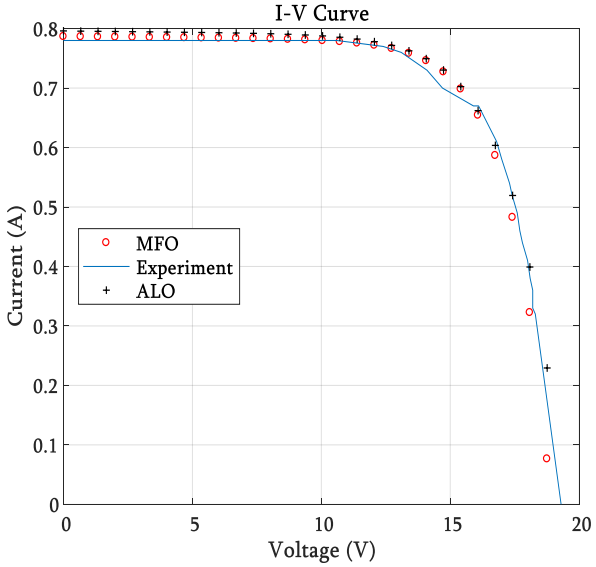

Figure 9 Comparison between the experimental and estimated I-V characteristic curve at T=37^{0}C and G=719.8Wm^{-2}. Date: 28/05/2018.

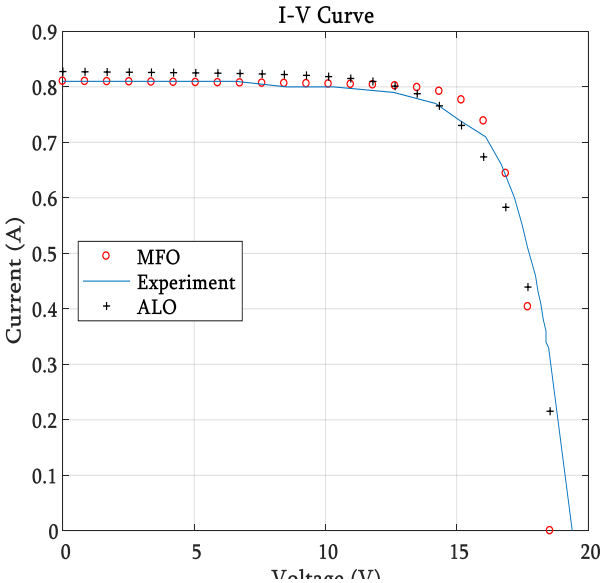

Figure 10 Comparison between the experimental and estimated I-V characteristic curve at T=39^{0}C and G=725.92Wm^{-2}. Date: 31/05/2018.

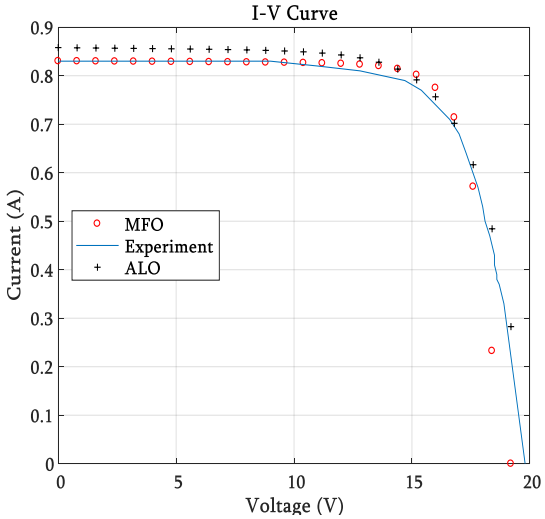

Figure 11 Comparison between the experimental and estimated I-V characteristic curve at T=40.90^{0}C and G=745.80Wm^{-2}. Date:04/06/18.

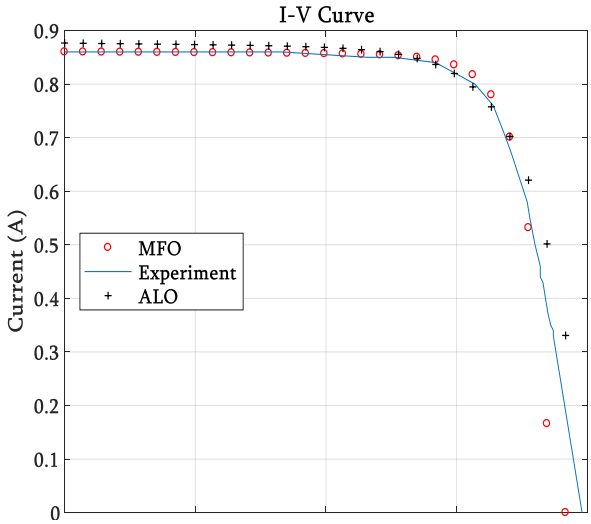

Figure 12 Comparison between the experimental and estimated I-V characteristic curve at T=45.50^{0}C and G=798.10Wm^{-2}. Date: 08/06/2018.

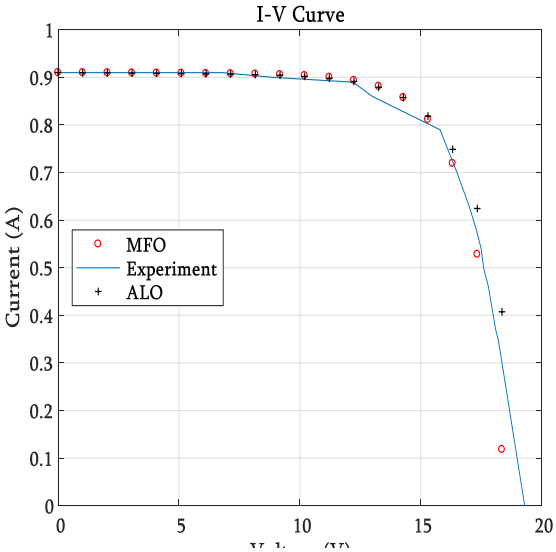

Figure 13 Comparison between the experimental and estimated I-V characteristic curve at T=46^{0}C and G=823.99Wm^{-2}. Date: 11/06/2018.

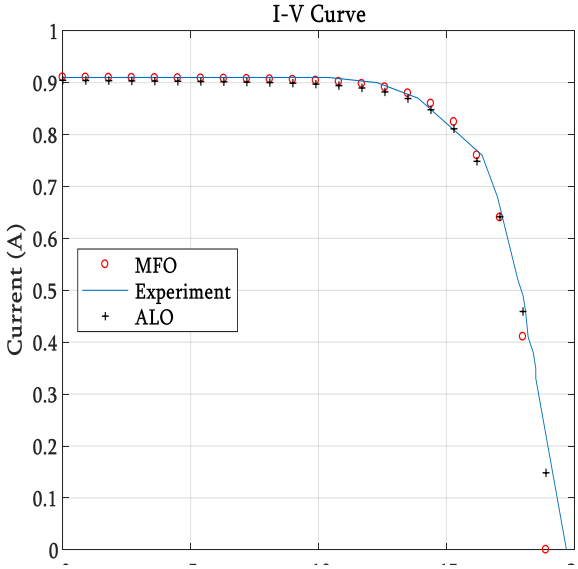

Figure 14 Comparison between the experimental and estimated I-V characteristic curve at T=47.98^{0}C and G=828.87Wm^{-2}. Date: 13/06/2018.

The calculated I-V curves from the MFO have shown better match with the measured I-V curves than that of the ALO, this shows that the MFO extracted parameters values are better than that of the ALO.To further illustrate the accuracy of thetechniques,statistical analyses were carried out for the two techniques and the reported errors are compared with the errors reported in [24] and [26]as shown in Table1.

TABLE 1 Comparison of MBE/MAE, RMSE, AE at MPP and R for both MFO and ALO at different Irradiance levels.

Author	Irradiance level	Model	Technique	R	MBE/ MAE	RMSE	AE at MPP
Ref. [26]	109.2Wm^{-2}	TDM	MFO	0.999	8.6E-07	0.0018	8.9E-05
	246.65Wm^{-2}			0.999	9.1E-07	0.0120	0.0023
	347.8Wm^{-2}			0.999	5.0E-07	0.0099	0.0203
	580.3Wm^{-2}			0.999	1.4E-06	0.0245	0.0304
Ref. [24]	-	SDM	ALO	-	0.001	2.5E-06	-
This research	719.8Wm^{-2}	TDM	MFO	0.833	0.198	0.261	0.021
			ALO	0.801	0.220	0.283	0.790
	725.92Wm^{-2}		MFO	0.874	0.146	0.211	0.028
			ALO	0.881	0.158	0.205	0.020
	745.80Wm^{-2}		MFO	0.908	0.119	0.172	0.045
			ALO	0.927	0.115	0.154	0.003
	798.10Wm^{-2}		MFO	0.859	0.162	0.225	0.004
			ALO	0.837	0.193	0.241	0.013
	823.99Wm^{-2}		MFO	0.848	0.173	0.238	0.017
			ALO	0.833	0.194	0.249	0.005
	828.87Wm^{-2}		MFO	0.909	0.123	0.172	0.028
			ALO	0.897	0.140	0.183	0.032

It can be observed that, the errors reported by the MFO technique are small compared to that of the ALO. But compared to the reported errors by the two techniques in the literature it was observed that, both the ALO and MFO have lost their accuracies with the increased number of the unknown parameters. This is because the reported errors by the MFO and ALO techniques in the literature are far much smaller than those reported in this research.However, the reported errorsfor this research for six different irradiance levels are compared graphically as shown in Fig. 15 to 18.

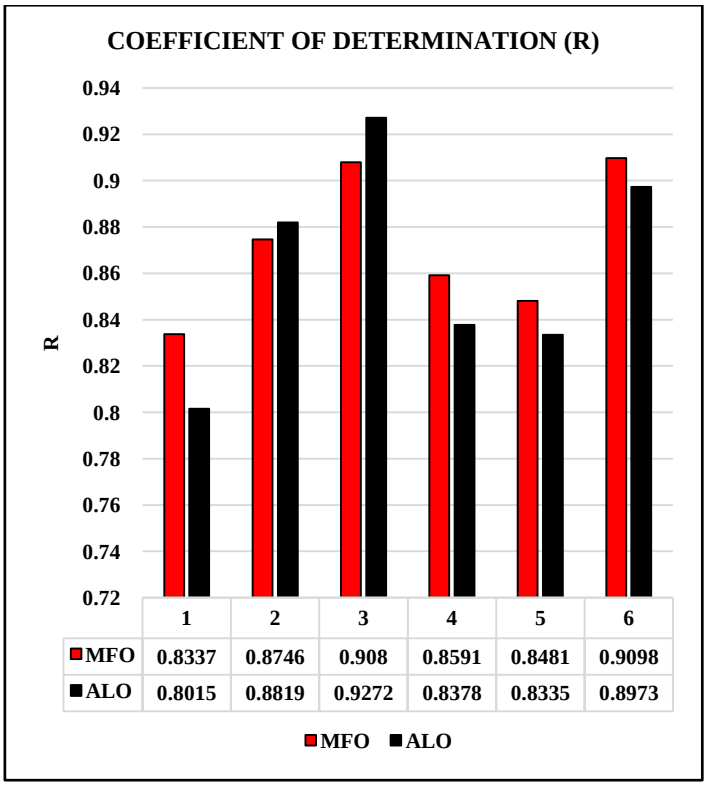

Figure 15 Comparison of R from both ALO and MFO simulated I-V curves.

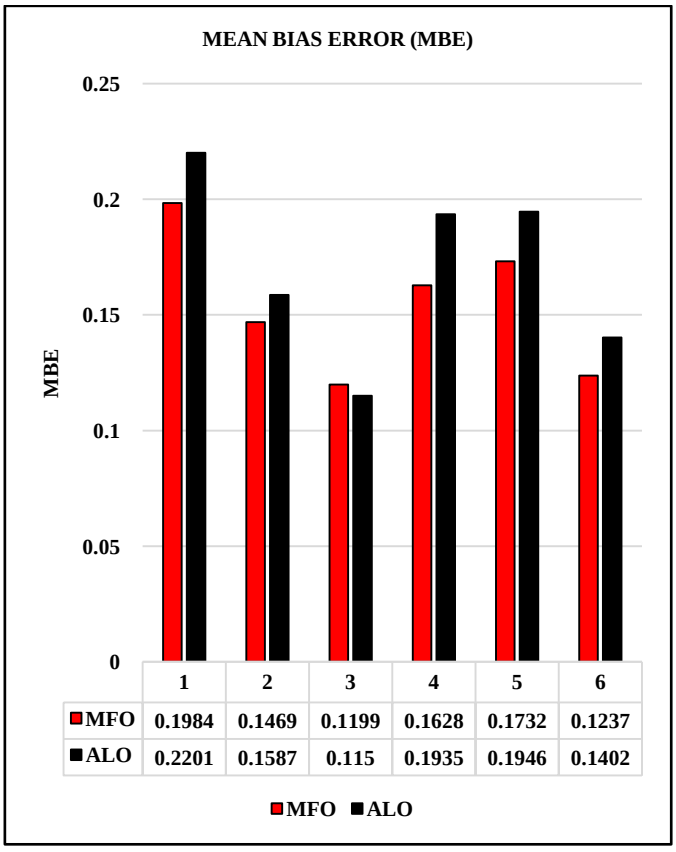

Figure 16 Comparison of MBE from both ALO and MFO simulated I-V curves.

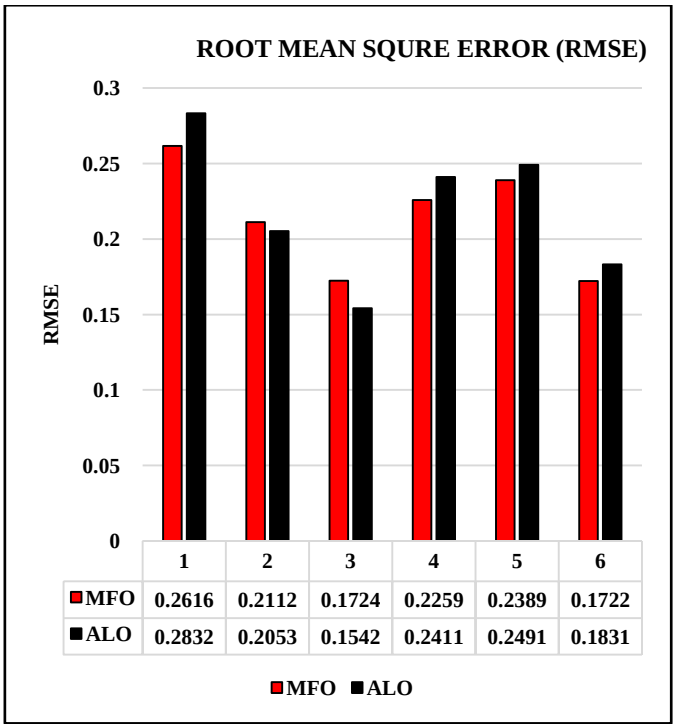

Figure 17 Comparison of RMSE form both ALO and MFO simulated I-V curves.

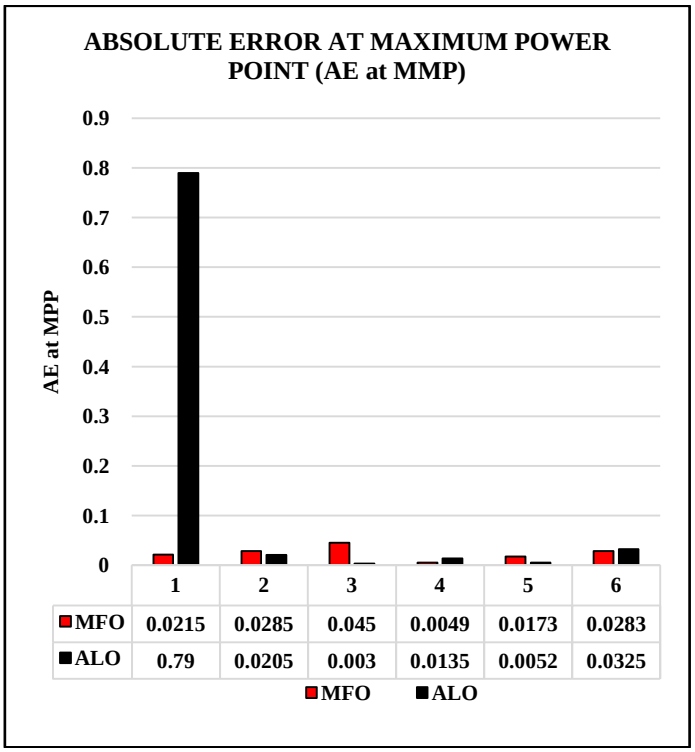

Figure 18 Comparison of AE at MPP from both ALO and MFO I-V curves.

Furthermore, the most important aspects of the comparison between the MFO algorithm and the ALO apart from accuracy are the speed of convergence and the execution time. Under the same parameter settings, Figure 19 to 24 shows thatthe MFO algorithm converges to the optimal solution rapidly compared to the ALO.However, Table 2 indicates that the execution time of ALO algorithm is about 18 times that of MFO technique.

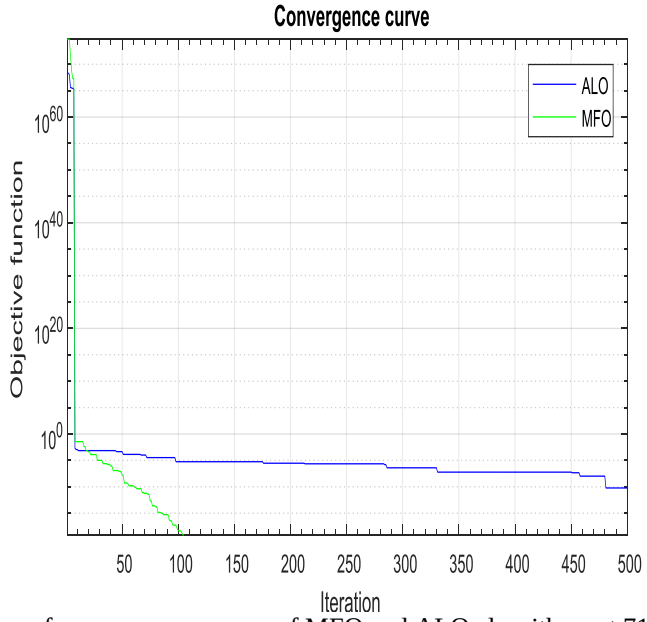

Figure 19 Comparison of convergence curves of MFO and ALO algorithms at 719.8Wm^{-2} and 37^{o}C.

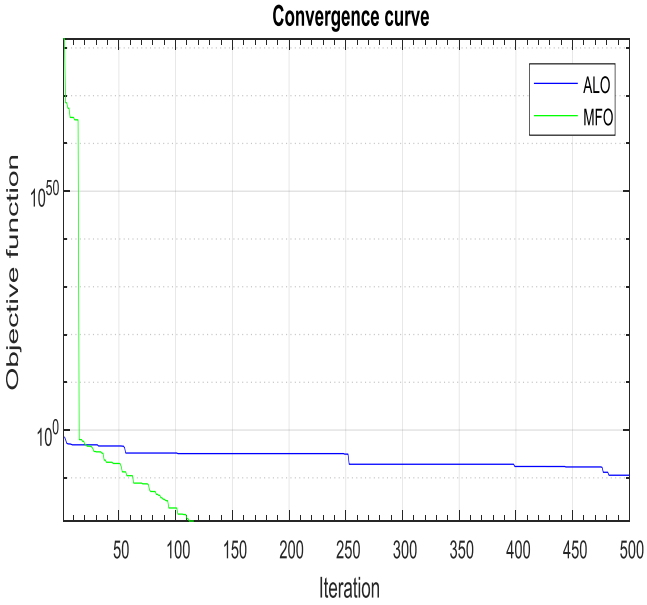

Figure 20 Comparison of convergence curves of MFO and ALO algorithms at 725.92Wm^{-2} and 39^{o}C.

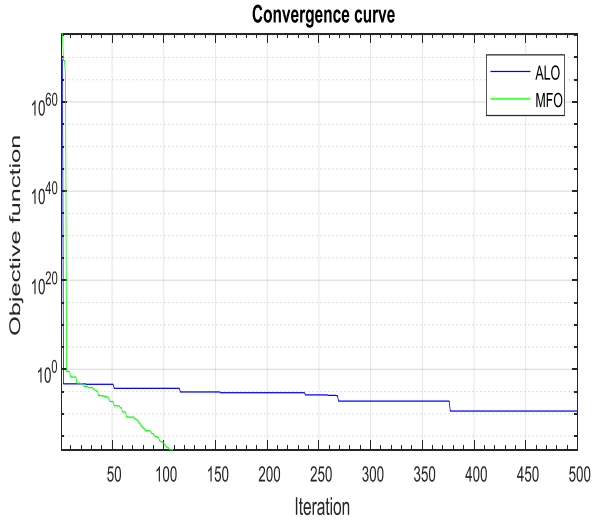

Figure 21 Comparison of convergence curves of MFO and ALO algorithms at 745.80Wm^{-2} and 40.90^{o}C.

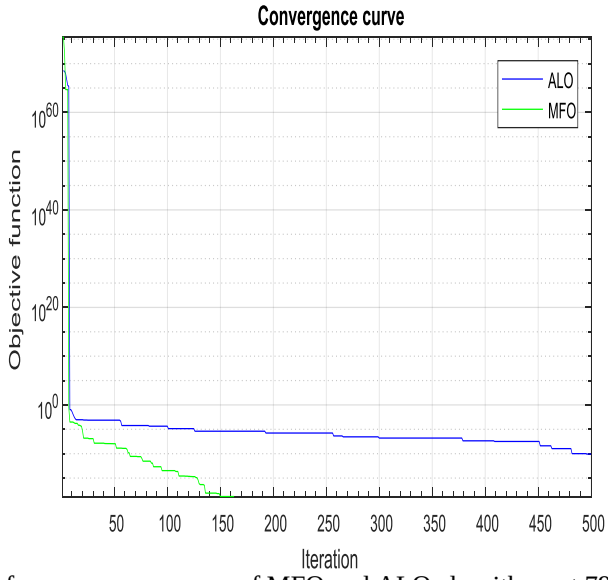

Figure 22 Comparison of convergence curves of MFO and ALO algorithms at 798.10Wm^{-2} and 45.50^{o}C.

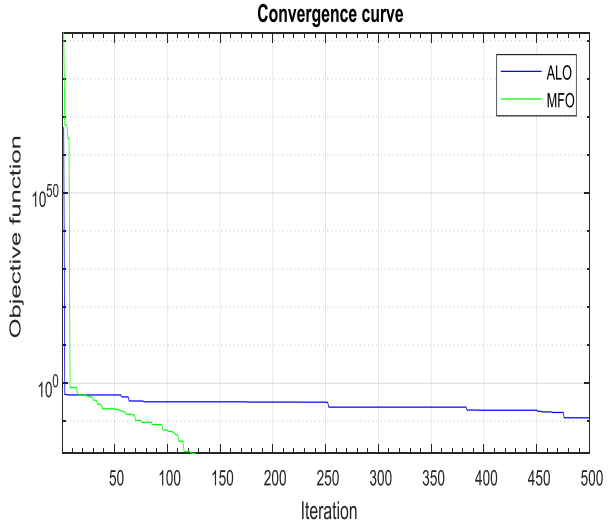

Figure 23 Comparison of convergence curves of MFO and ALO algorithms at 823.99Wm^{-2} and 47.80^{o}C.

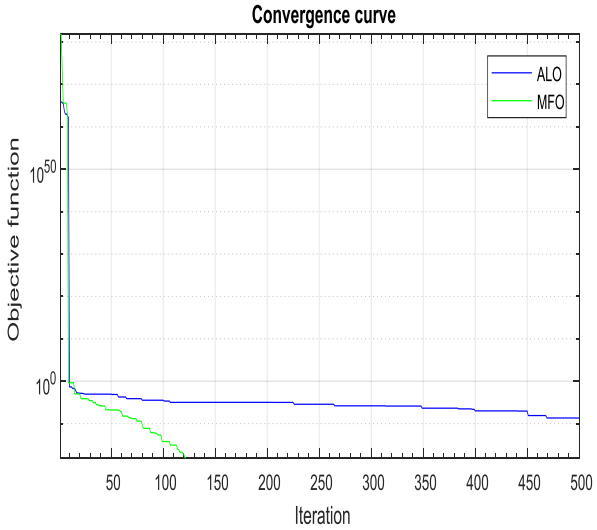

Figure 24 Comparison of convergence curves of MFO and ALO algorithms at 828.87Wm^{-2} and 47.98^{o}C.

TABLE 2 Execution time consumed by each Algorithm for a single run

Algorithm	Execution time (sec)
MFO	152.2288
ALO	2254.1822

The optimal values of the TDM extracted parameters by the ALO and MFO at different level of irradiance and temperature are given in Table 3.

TABLE 3 Extracted parameters of the TDM of AP-PM-20 (20W) Polycrystalline PV module by MFO and ALO algorithms at different levels of Irradiance and Temperature.

Date, Irradiance G & Temperature T levels.	Algorithm	Parameters								
		Rs (Ω)	Rp (Ω)	Io1 (A)	Io2 (A)	Io3 (A)	a1	a2	a3	Iph (A)
28/05/18, G = 719.80W/m^2, T = 37.00^{0}C	MFO	0.0682	2521.5	7.66E-10	4.37E-06	6.00E-06	0.9819	1.4787	3.0355	0.7865
	ALO	0.3624	2419.2	6.78E-10	6.45E-06	7.13E-06	0.6596	1.1218	2.7640	0.7960
31/05/18, G = 725.92W/m^2, T = 39.00^{0}C	MFO	0.0171	2251.6	6.58E-10	7.31E-07	7.28E-06	0.7864	1.5304	3.1637	0.8100
	ALO	0.3511	2474.2	5.19E-10	7.08E-06	4.81E-06	0.4701	1.8580	2.9857	0.8275
04/06/18, G = 745.80W/m^2, T = 40.90^{0}C	MFO	0.0692	3386.0	2.71E-10	8.32E-07	3.43E-06	0.7720	1.4413	3.4755	0.8300
	ALO	0.3317	2140.5	4.24E-10	6.54E-06	3.81E-06	0.3817	1.52716	2.0693	0.8580
08/06/18, G = 798.10W/m^2, T = 45.50^{0}C	MFO	0.0274	3683.6	4.43E-10	2.00E-06	2.63E-06	0.8433	1.7092	2.8761	0.8600
	ALO	0.4526	1911.8	2.07E-10	6.06E-06	3.91E-06	0.8430	1.7255	2.6507	0.8766
11/06/18, G = 823.99W/m^2, T = 47.80^{0}C	MFO	0.0008	4009.7	8.94E-10	6.78E-06	3.31E-06	0.9614	1.6401	3.2007	0.9100
	ALO	0.3956	2871.5	6.89E-10	3.97E-06	5.39E-06	0.8449	1.1023	3.3170	0.9101
13/06/18, G = 828.87W/m^2, T = 47.98^{0}C	MFO	0.0040	3106.5	3.95E-10	6.09E-06	6.54E-06	0.9635	1.6958	2.5903	0.9100
	ALO	0.0450	2634.8	3.78E-10	4.17E-06	6.77E-06	0.6382	1.1567	2.8041	0.9045

V. Conclusion

From the results obtained, both the two techniques were found to have slightly the same level of accuracy although the MFO have slightly recorded the least average value of; MBE as 0.15, RMSE as 0.21, AE at MPP as 0.022 and best value of R as 87% over the ALO with MBE 0.17, RMSE 0.22, AE at MPP 0.14 and R as 86%. However, in terms of execution time MFO algorithm have outstandingly outperforms the ALO having recorded the execution time of 152.2288 seconds for a single run while the ALO recorded 2254.1824 seconds for the same number of run, this indicates that MFO is about 15 times faster than ALO. Moreover, in terms of

speed of convergence MFO outperforms the ALO. However, the two techniques were found to slightly lose their accuracies with the increased number of the unknown electrical parameters especially towards the V_{oc} point. Thus, for accurate and efficient parameters extraction of a TDM of a PV module, MFO algorithm outperforms ALO algorithm based on this research. The knowledge of the extracted parameters is used not only to improve design and evaluate performance of PV cells but also to extract the MPP of the PV module and array. However, to find more suitable materials for high conversion efficiency of PV cell, it is important to extract the electrical unknown parameters of the present design for further improvement

Acknowledgment

The authors wish to acknowledge the contributions of Associate Prof. M. H. Ali, Department of Physics, Faculty of Physical Sciences, Bayero University Kano, Nigeria and Dr. H. A. Bashir,Department of Electrical Engineering, Faculty of Engineering,Bayero University Kano, Nigeria.

References

[1]. K. Bouzidi, M. Chegaar, and M. Aillerie, "Solar cells parameters evaluation from dark I-V characteristics," *Energy Procedia*, vol. 18, no. 1, pp. 1601–1610, 2012.
[2]. M. A. Green, Y. Hishikawa, A. W. Y. Ho-Baillie, E. D. Dunlop, and D. H. Levi, "Solar cell efficiency tables (version 51)," *Wiley Prog. Photovolt*, no. November 2017, pp. 3–12, 2018.
[3]. F. Z. Zerhouni, M. H. Zerhouni, M. T. Benmessaoud, A. B. Stambouli, and O. E. M. Naouer, "Proposed Methods to Increase the Output Efficiency of a Photovoltaic (PV) System," *Acta Polytchnica Hungarica*, vol. 7, no. 2, pp. 55–70, 2010.
[4]. W. Li *et al.*, "Six-parameter electrical model for photovoltaic cell / module with compound parabolic concentrator," *Sol. Energy*, vol. 137, pp. 551–563, 2016.
[5]. V. Jack, Z. Salam, and K. Ishaque, "Cell modelling and model parameters estimation techniques for photovoltaic simulator application : A review," *Appl. Energy*, vol. 154, no. September, pp. 500–519, 2015.
[6]. M. H. Ali and J. M. Olayinka, "Comparative Study of Diferential Evolution and Global Maximum Optimization Techniques," *5th Int. Conf. Sch. Sci. Technol. Educ. (SSTE), FUT,Minna.*, pp. 226–236, 2017.
[7]. V. Tamrakar, S. . Gupta, and Y. Sawle, "Single-Diode and Two-Diode Pv Cell Modeling Using Matlab For Studying Characteristics Of Solar Cell Under Varying Conditions," *Electr. Comput. Eng. An Int. J.*, vol. 4, no. 2, pp. 67–77, 2015.
[8]. R. Abbassi, A. Abbassi, M. Jemli, and S. Chebbi, "Identi fi cation of unknown parameters of solar cell models : A comprehensive overview of available approaches," *Renew. Sustain. Energy Rev.*, vol. 90, no. February, pp. 453–474, 2018.
[9]. M. Khalis, R. Masrour, Y. Mir, and M. Zazoui, "Two methods for extracting the parameters of a non-ideal diode," *Int. J. Phys. Sci.*, vol. 10, no. 8, pp. 270–275, 2015.
[10]. M. . Ali and Y. Abdullahi, "Parameter Extraction and Estimation Based on the PV Panel Outdoor Performance Using Iterative Method," *Bayero J. Pure Appl. Sci.*, vol. 10, no. 1, pp. 362–367, 2016.
[11]. M. Zagrouba, A. Sellami, and M. Bouaı, "Identification of PV solar cells and modules parameters using the genetic algorithms : Application to maximum power extraction," *Sol. Energy*, vol. 84, pp. 860–866, 2010.
[12]. X. Lingyun, S. Lefei, H. Wei, and J. Cong, "Solar Cells Parameter Extraction Using a Hybrid Genetic Algorithm," in *2011 Third International Conference on Measuring Technology and Mechatronics Automation*, 2011, no. 1, pp. 1–4.
[13]. N. Moldovan, R. Picos, and E. Garcia-moreno, "Parameter Extraction of a Solar Cell Compact Model usign Genetic Algorithms," in *Proceedings of the 2009 Spanish Conference on Electron Devices - Feb 11-13, 2009. Santiago de Compostela, Spain. Parameter*, 2009, vol. 00, no. C, pp. 379–382.
[14]. J. A. Jervase, H. Bourdoucen, and A. Al-lawati, "Solar cell parameter extraction using genetic algorithms," *IOP Conf. Ser. Mater. Sci. Eng.*, vol. 1922, 2001.
[15]. M. R. Alrashidi and M. F. Alhajri, "Solar Cell Parameters Estimation Using Simulated Annealing Algorithm," *World Acad. Sci. Eng. Technol. Int. J. Electr. Comput. Eng.*, vol. 7, no. 4, pp. 370–373, 2013.
[16]. S. Asif and Y. Li, "Solar Cell Modeling and Parameter Optimization," *J. Propuls. POWER*, vol. 24, no. 5, 2008.
[17]. V. Khanna, B. K. Das, D. Bisht, and P. K. Singh, "A three diode model for industrial solar cells and estimation of solar cell parameters using PSO algorithm," *Renew. Energy*, vol. 78, pp. 105–113, 2015.
[18]. A. Harrag and S. Messalti, "Three, Five and Seven PV Model Parameters Extraction using PSO," *Energy Procedia*, vol. 119, pp. 767–774, 2017.
[19]. L. Hui and L. Shi, "Parameters Identification of Photovoltaic Cells Based on Differential Evolution Algorithm," in *ITM Web of Conferences 7*, 2016, vol. 04003, pp. 0–4.
[20]. K. Ishaque, Z. Salam, S. Mekhilef, and A. Shamsudin, "Parameter extraction of solar photovoltaic modules using penalty-based differential evolution," *Appl. Energy*, vol. 99, pp. 297–308, 2012.
[21]. R. Tamrakar and A. Gupta, "Extraction of Solar Cell Modelling Parameters Using Differential Evolution Algorithm," *Ijireeice*, vol. 3, no. 11, pp. 78–82, 2015.
[22]. M. Louzazni, A. Khouya, K. Amechnoue, A. Crăciunescu, and M. Mussetta, "Comparative prediction of single and double diode parameters for solar cell models with firefly algorithm," *2017 10th Int. Symp. Adv. Top. Electr. Eng. ATEE 2017*, pp. 860–865, 2017.
[23]. C. Saravanan and K. Srinivasan, "Optimal Extraction of Photovoltaic Model Parameters Using Gravitational Search Algorithm Approach," *circuit Syst.*, vol. 7, pp. 3849–3861, 2016.
[24]. G. Kanimozhi, R. Rajathy, and H. Kumar, "Estimation of maximum power point in photovoltaic cell based on parameters identification approach by Ant Lion Optimizer implemented in IPython," *Spec. Issue Int. J. Comput. Sci. Inf. Secur.*, vol. 14, no. Cic, pp. 44–51, 2016.
[25]. M. R. Alrashidi, M. F. Alhajri, and K. M. El-Naggar, "Parameters Estimation of Double Diode Solar Cell Model," *Eng. Technol.*, vol. 7, no. 2, pp. 93–96, 2013.
[26]. D. Allam, D. A. Yousri, and M. B. Eteiba, "Parameters extraction of the three diode model for the multi-crystalline solar cell / module using Moth-Flame Optimization Algorithm," *Energy Convers. Manag.*, vol. 123, pp. 535–548, 2016.
[27]. T. Selmi, M. Abdul-niby, and M. Alameen, "Analysis and Investigation of a Two-Diode Solar Cell Using MATLAB / Simulink," *Int. J. Renew. Energy Res.*, vol. 4, no. 1, pp. 99–102, 2014.
[28]. K. Ishaque and Z. Salam, "A comprehensive MATLAB Simulink PV system simulator with partial shading capability based on

two-diode model," *Sol. Energy*, vol. 85, no. 9, pp. 2217–2227, 2011.
[29]. T. Ahmad, S. Sobhan, and F. Nayan, "Comparative Analysis between Single Diode and Double Diode Model of PV Cell : Concentrate Different Parameters Effect on Its Efficiency," *J. Power Energy Eng.*, vol. 4, no. March, pp. 31–46, 2016.
[30]. S. Nahla, N. Yahaya, and B. Singh, "Single-diode model and two-diode model of PV modules : A comparison," in *IEEE International Conference on Control System, Computing and Engineering*, 2013, no. November.
[31]. S. Mirjalili, "Knowledge-Based Systems Moth-flame optimization algorithm : A novel nature-inspired heuristic paradigm," *Knowledge-Based Syst.*, vol. 89, pp. 228–249, 2015.
[32]. S. Mirjalili, "Advances in Engineering Software The Ant Lion Optimizer," *Adv. Eng. Softw.*, vol. 83, pp. 80–98, 2015.
[33]. R. P. Vengatesh and S. E. Rajan, "Investigation of cloudless solar radiation with PV module employing Matlab – Simulink," *Sol. Energy*, vol. 85, no. 9, pp. 1727–1734, 2011.

A. M. Nura, " Comparative Study Between Moth Flame And Ant-Lion Optimization Techniques Using Parameter Extraction Of A Three Diode Model Of A Photovoltaic Module.." IOSR Journal of Applied Physics (IOSR-JAP) , vol. 11, no. 4, 2019, pp. 01-21.